arXiv:cond-mat/0207101v1 [cond-mat.soft] 3 Jul 2002

Pattern forming instability induced by light in pure and dye-doped nematic liquid crystals

D.O. Krimer, G. Demeter,* and L. Kramer
Physikalisches Institut der Universität Bayreuth, D-95440 Bayreuth, Germany
(Dated: January 7, 2022)

We study theoretically the instabilities induced by a linearly polarized ordinary light wave incident at a small oblique angle on a thin layer of homeotropically oriented nematic liquid crystal with special emphasis on the dye-doped case. The spatially periodic Hopf bifurcation that occurs as the secondary instability after the stationary Freedericksz transition is analyzed.

I. INTRODUCTION

Liquid crystals (LCs) are known to demonstrate a very rich variety of interesting optical phenomena which have been studied intensively during the last two decades. A nematic LC behaves optically as a uniaxial anisotropic medium with the optical axis along the local molecular orientation described by the director $\mathbf{n}(\mathbf{r},t)$. Moreover, when light propagates through the nematic, its electric field exerts a torque on the molecules which can induce molecular reorientation. When there is only an ordinary wave in the LC (polarization perpendicular to the plane containing the optical axis and wavevector), the initial distribution of the director becomes unstable when the intensity of light reaches a certain critical value. This is the so-called Light Induced Freedericksz Transition (LIFT). The director reorientation leads to a change of birefringence and, as a consequence, the polarization is changed as light propagates through the layer [1, 2].

It is known [3, 4] that a periodic equilibrium configuration of the nematic director can appear in a thin-film LC in the magnetic or electric field induced Freedericksz transition under certain conditions. Our work is devoted to the search of analogous phenomena in the LIFT of nematic LCs including the dye-doped case. We will show that the Hopf bifurcation that occurs as a secondary bifurcation after the LIFT leads indeed to a periodic pattern, although the mechanism is here quite different (see Conclusions). Doping is important because the LIFT threshold of a dye-doped nematic can be two orders of magnitude smaller than for a pure nematic. The nature of this anomalously low threshold was the subject of numerous studies (see [5, 6] and references therein). The fact that the threshold intensity is low allows the spot size of the light to be much larger than the thickness of the layer, thus a large aspect ratio system can be realized.

This paper is organized as follows. In Sec. II we present the theoretical description of our problem. In Sec. III we perform the linear stability analysis of the homeotropic state which gives the threshold for the LIFT. The numerical method of calculating the stationary distorted state is described in Sec. IV. Finally, in Sec. V, we do the linear stability analysis of the stationary distorted state with respect to general perturbations in the plane of the nematic layer.

II. THEORETICAL MODEL

We consider a linearly-polarized plane wave incident at a small oblique angle β_0 on a layer of dye-doped nematic LC which has initially homeotropic alignment (see Fig. 1). The light is polarized along the y-axis i.e., we deal with an ordinary wave. Strong anchoring of the nematic at the boundaries of the layer is assumed. The optical torque acting on the director is given by $\tau = \xi_{eff}/16\pi(\mathbf{n}\cdot\mathbf{E}^*)(\mathbf{n}\times\mathbf{E}) + c.c.$, where $\mathbf{E}$ is the amplitude of the optical electric field, $\xi_{eff} = \varepsilon_a + \zeta$. $\varepsilon_a = \varepsilon_\parallel - \varepsilon_\perp$ is the dielectric anisotropy and $\varepsilon_\perp$ ($\varepsilon_\parallel$) is the dielectric permittivity (at optical frequency) perpendicular (parallel) to $\mathbf{n}$. ζ phenomenologically describes the effect of certain dye dopants ($\xi_{eff} = \varepsilon_a$ in a pure LC) and can be both positive and negative and depends on dye concentration, molecular structures of both host and dye materials, on the wavelength of light, and on the temperature [5, 6]. Obviously, the electrical part of the free energy will contain the same factor ξ_{eff}. The density of the free energy of the dye-doped nematic LC is thus assumed in the form:

$$F = F_{elastic} - \frac{\xi_{eff}}{16\pi} \mid \mathbf{n}\cdot\mathbf{E} \mid^2, \tag{1}$$

where $F_{elastic} = K_1/2\,(\nabla\cdot\mathbf{n})^2 + K_2/2\,(\mathbf{n}\cdot\nabla\times\mathbf{n})^2 + K_3/2\,(\mathbf{n}\times\nabla\times\mathbf{n})^2$ is the standard Frank free energy density and K_1, K_2, K_3 are respectively the splay, twist and bend elastic constants of the LC [7].

We first assume that the director components depend only on z,t. We introduce the angles $\theta(z,t)$ and $\varphi(z,t)$ (see Fig.1) so that $\mathbf{n} = (\sin\theta, \cos\theta\sin\varphi, \cos\theta\cos\varphi)$. Using the standard variational principle [1] and taking the dissipation function in the form $R = \frac{\gamma}{2}\dot{\mathbf{n}}^2$, where γ is an effective rotational viscosity, the equations of motion for $\theta(z,t)$ and $\varphi(z,t)$ can be derived.

In addition we need Maxwell's equations to determine the electric field. These equations contain the complex

*on leave from the Research Institute for Particle and Nuclear Physics of the Hungarian Academy of Sciences, Budapest, Hungary.

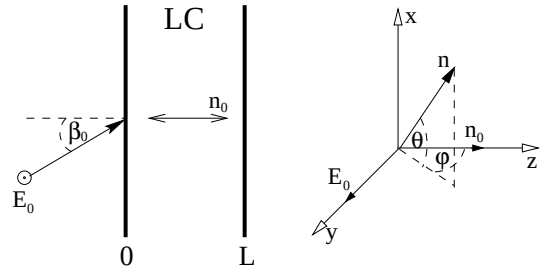


FIG. 1: Geometry of the setup: linearly polarized light along the **y**-direction incident at angle β_0 on a nematic LC layer with the director $\mathbf{n_0} \parallel \mathbf{z}$ (homeotropic state). The components of the director **n** are described in terms of the angles θ, φ ($\theta = \varphi = 0$ in the homeotropic state).

dielectric tensor which depends on the director components:

$$\varepsilon_{ij} = (\varepsilon_\perp + i\gamma_\perp)\,\delta_{ij} + (\varepsilon_a + i\gamma_a)\,n_i n_j. \tag{2}$$

In (2) $\gamma_a = \gamma_\perp - \gamma_\parallel$, where $\gamma_\perp$ and $\gamma_\parallel$ are the imaginary parts of the dielectric permittivity for **E** perpendicular and parallel to **n** respectively. They describe the absorption effect by the dye, so they vanish in pure LCs. The magnetic anisotropy at optical frequencies can be neglected. Since the components of the dielectric tensor depend on the z-coordinate only, we may use the stratified medium approach for describing wave propagation [2]. We write the electric and magnetic fields in the form: $\mathbf{E}(\mathbf{r},t) = 1/2(\mathbf{E}(z,t)e^{is_0k_0x}e^{-i\omega t} + c.c.), \mathbf{H}(\mathbf{r},t) = 1/2(\mathbf{H}(z,t)e^{is_0k_0x}e^{-i\omega t} + c.c.)$, where $k_0 = \omega/c$ is the wavenumber in vacuum and $s_0 = \sin(\beta_0)$. Here $\mathbf{E}(z,t), \mathbf{H}(z,t)$ are amplitudes that vary slowly in time compared to ω^{-1} and obey the equation:

$$\frac{d\bar{\Psi}}{dz} = ik_0 \mathsf{D}\bar{\Psi}, \tag{3}$$

where

$$\bar{\Psi} = \begin{pmatrix} E_x \\ H_y \\ E_y \\ -H_x \end{pmatrix} \tag{4}$$

and

$$\mathsf{D}(z) = \begin{pmatrix} -\frac{\varepsilon_{xz}s_0}{\varepsilon_{zz}} & 1 - \frac{s_0^2}{\varepsilon_{zz}} & -\frac{\varepsilon_{yz}\,s_0}{\varepsilon_{zz}} & 0 \\ \varepsilon_{xx} - \frac{{\varepsilon_{xz}}^2}{\varepsilon_{zz}} & -\frac{\varepsilon_{xz}\,s_0}{\varepsilon_{zz}} & \varepsilon_{xy} - \frac{\varepsilon_{xz}\,\varepsilon_{yz}}{\varepsilon_{zz}} & 0 \\ 0 & 0 & 0 & 1 \\ \varepsilon_{xy} - \frac{\varepsilon_{xz}\,\varepsilon_{yz}}{\varepsilon_{zz}} & -\frac{\varepsilon_{yz}\,s_0}{\varepsilon_{zz}} & \varepsilon_{yy} - \frac{{\varepsilon_{yz}}^2}{\varepsilon_{zz}} - s_0^2 & 0 \end{pmatrix}. \tag{5}$$

The z-component of the electric field can be found from the following relation:

$$E_z = -\frac{s_0}{\varepsilon_{zz}}H_y - \frac{\varepsilon_{xz}}{\varepsilon_{zz}}E_x - \frac{\varepsilon_{yz}}{\varepsilon_{zz}}E_y. \tag{6}$$

We will examine the case $\xi_{eff} > 0$ so that the preferred orientation corresponds to the director parallel to the electric field $\mathbf{n}||\mathbf{E}$. Since in our geometry initially $\mathbf{n} \perp \mathbf{E}$, the homeotropic state will cease to be stable above some critical intensity of the incident light. The reorientation of the LC leads to modification of the electric field polarization inside the LC owing to the fact that it becomes an inhomogeneous anisotropic medium.

III. STABILITY ANALYSIS OF THE HOMEOTROPIC STATE

We first perform the linear stability analysis of the homeotropic state ($\theta = \varphi = 0$). The linearized equation of motion for $\varphi(z,t)$ has the following simple form:

$$\gamma\partial_t\varphi = K_3\partial_z^2\varphi + \frac{(\varepsilon_a + \zeta)}{16\pi}(2 \mid E_{0y} \mid^2 \varphi + E_{1z}^* E_{0y} + E_{1z}E_{0y}^*). \tag{7}$$

Here E_{0y} is the y-component of the electric field amplitude for the undistorted nematic (homeotropic orientation) and E_{1z} is the z-component of the field that is caused by nematic reorientation (calculated to the first order in φ). It is easily seen that in the undistorted LC the light maintains its polarization inside the layer, so that we have only one nonzero component of the electric field $E_{0y}(z) = E_0 e^{ik_z z}$, where $k_z = k_{Re} + ik_{Im} \simeq k_0\sqrt{\varepsilon_\perp - s_0^2} + i\gamma_\perp k_0/(2\sqrt{\varepsilon_\perp - s_0^2})$ (terms of the order of $\left(\gamma_\perp/(\varepsilon_\perp - s_0^2)\right)^2$ in k_z are neglected because $\gamma_\perp \ll \varepsilon_\perp$) and E_0 is the amplitude of the incident electric field. In the linear approximation θ remains zero. Straightforward calculations yield the following equation for $E_{1z}(z)$ from Eqs. (3-6):

$$\begin{aligned}&(\varepsilon_\perp + \varepsilon_a + i(\gamma_a + \gamma_\perp))\frac{d^2E_{1z}}{dz^2} + k_0^2(\varepsilon_\perp + i\gamma_\perp) \\ &\times(\varepsilon_\perp + \varepsilon_a - s_0^2 + i(\gamma_a + \gamma_\perp))E_{1z} + k_0^2(\varepsilon_a + i\gamma_a) \\ &\times(\varepsilon_\perp + i\gamma_\perp)\varphi E_{0y} + (\varepsilon_a + i\gamma_a)\frac{d^2(\varphi E_{0y})}{dz^2} = 0\end{aligned} \tag{8}$$

Substituting $E_{1z}(z)$ into (8) in the form $E_{1z}(z) = E(z)e^{ik_z z}$ and taking into account that $k_0 L \gg 1$ (L is the width of the layer), a first-order ODE for $E(z)$ can be derived. Keeping in mind that $E_{1z}(0) = 0$ we eventually obtain from Eqs. (7,8) the following integro-differential equation for φ:

$$\begin{aligned}&\tau\frac{\partial\varphi(z,t)}{\partial t} = \left(\frac{L}{\pi}\right)^2\frac{\partial^2\varphi(z,t)}{\partial z^2} + \rho\left\{\left(\frac{\pi\kappa}{L}\right)\right. \\ &\times\int_0^z\left[\psi\cos\left(\frac{\pi\kappa}{L}(z'-z)\right) + \sin\left(\frac{\pi\kappa}{L}(z'-z)\right)\right] \\ &\left.\times e^{\frac{\pi}{L}\xi\kappa(z'-z)}\varphi(z',t)dz' + \varphi(z,t)\right\}e^{-2k_{Im}z},\end{aligned} \tag{9}$$

where ψ, ξ, κ and τ are parameters defined as:

$$\psi = -\frac{\varepsilon_a^2\gamma_\perp - 3\varepsilon_a\varepsilon_\perp\gamma_\perp + 2\gamma_a\varepsilon_\perp^2 - 2\gamma_a\varepsilon_\perp\varepsilon_a}{2\,(\varepsilon_a + \varepsilon_\perp)\,\varepsilon_a\varepsilon_\perp},$$

$$\xi = \frac{2\gamma_a\varepsilon_\perp^2 - 3\varepsilon_a\varepsilon_\perp\gamma_\perp - \varepsilon_a^2\gamma_\perp}{2\left(\varepsilon_a+\varepsilon_\perp\right)\varepsilon_a\varepsilon_\perp}$$

$$\kappa = \frac{L}{\pi}\frac{s_0^2\varepsilon_a k_0}{2\sqrt{\varepsilon_\perp}(\varepsilon_\perp+\varepsilon_a)},\ \tau = \frac{\gamma L^2}{\pi^2 K_3}$$

In the parameters defined above only the linear terms in $\gamma_a, \gamma_\perp$ were kept ($\gamma_a, \gamma_\perp \ll 1$). The parameter τ is the characteristic time of the director motion and $\rho = I/I_c$, where I is the intensity of the incident light and I_c is defined as:

$$I_c = \frac{\pi^2}{L^2}\frac{c(\varepsilon_\perp+\varepsilon_a)K_3}{\varepsilon_a\sqrt{\varepsilon_\perp}\eta},\ \eta = (\varepsilon_a+\zeta)/\varepsilon_a \qquad (10)$$

I_c coincides with the threshold intensity of the LIFT for a pure nematic ($\eta = 1$, $\gamma_\perp = \gamma_\parallel = 0$) at perpendicular incidence [2]. Then Eq. (9) reduces to one obtained in [8].

We use a two-mode expansion with respect to z for the angle φ with the boundary conditions $\varphi(z=0) = \varphi(z = L) = 0$: $\varphi(z,t) = A_1(t)\sin(\pi z/L) + A_2(t)\sin(2\pi z/L)$, where A_1 and A_2 are time-dependent amplitudes. This is motivated by the fact that the distorted state is asymmetric with respect to the center of the layer because of absorption and the perturbation of the light polarization inside the layer. Therefore we have to include at least one mode that is symmetric and one mode that is antisymmetric with respect to the center of the layer. After projecting Eq.(9) onto the trial functions we have a system of two equations for the modes A_1 and A_2:

$$\tau\frac{dA_1}{dt} = \mathcal{L}_{11}A_1 + \mathcal{L}_{12}A_2,\ \tau\frac{dA_2}{dt} = \mathcal{L}_{21}A_1 + \mathcal{L}_{22}A_2, \qquad (11)$$

where the elements of the matrix $\mathcal{L}_{ij}$ depend on material parameters and the control parameters ρ and κ (which is proportional to s_0^2). We look for solutions proportional to $exp(\sigma t)$, where σ is the growth rate. The procedure of deriving $\mathcal{L}_{ij}$ is straightforward but the expressions for these elements are too long to be presented here.

The stability diagram in the (κ, ρ) plane can now be calculated for any given material parameters of the LC. As an example we consider the nematic 5CB doped with the dye AD1 at 0.1% concentration. We used the following values of material parameters at the temperature $T = 24°$: $\alpha_o = 42\ cm^{-1}$, $n_o = 1.53$, $\alpha_e = 190\ cm^{-1}$, $n_e = 1.71$, (absorption coefficients and refractive indices of the ordinary and extraordinary light, respectively), $\lambda = 633\ nm$ (wavelength of laser), $\zeta = 58$ [6], $\gamma = 0.845\ dyn\cdot s/cm^2$, $K_1 = 0.64\cdot 10^{-6}\ dyn$, $K_2 = 0.42\cdot 10^{-6}\ dyn$, $K_3 = 0.86\cdot 10^{-6}\ dyn$ [9] ; the calculations are made for a layer of 50 μm thickness. For these parameters $I_c = 33.21\ W/cm^2$, $\tau = 2.49\ s$. It is easy to show the following relations: $\gamma_\perp \simeq \alpha_o n_o/k_0$, $\gamma_a \simeq (\alpha_e n_e - \alpha_o n_o)/k_0$, $\varepsilon_\perp \simeq n_o^2$, $\varepsilon_a \simeq n_e^2 - n_o^2$ (neglecting terms of the order $\left(\gamma_\perp/(\varepsilon_\perp - s_0^2)\right)^2$).

The stability diagram is depicted in Fig. 2a. The solid line corresponds to a stationary bifurcation ($Re(\sigma) = Im(\sigma) = 0$) and the dashed one corresponds to a Hopf bifurcation of the homeotropic state ($Re(\sigma) = 0, Im(\sigma) \neq 0$). These lines divide the (κ, ρ) plane into a stable and an unstable region of the homeotropic alignment. They join in a so called Takens-Bogdanov point where $det(\mathcal{L}) = Tr(\mathcal{L}) = 0$.

There are two differences compared to the case of a pure LC. First, the enhancement of the orientational optical nonlinearity described by the parameter ζ leads to a "renormalization" of the threshold intensity (see Eq. (10)). (However, since Fig. 2a is plotted with the renormalized threshold intensity, this does not change the appearance of the stability diagram). Second, absorption gives rise to the attenuation of the field inside the nematic. This results in a shift of the line of primary instability to the region of higher intensities as is shown in Fig. 2b. From this figure one can see the quantitative difference between the case when the absorption is neglected (dot-dashed lines) and when the absorption is taken into account (solid and dashed lines). Note that the critical intensity ρ_{th} for perpendicular incidence thus becomes larger than 1.

It must be noted that we supposed that the nematic is maintained at constant temperature. Actually, due to the presence of the absorbing dye, the nematic will be heated by the light [10]. We have estimated the maximum temperature difference occurring *inside* the nematic 5CB doped with the dye AD1 from the steady-state heat conductivity equation (one-dimensional since we considered a plane wave). For the range of intensities $I = 30 - 100\ W/cm^2$ this difference was found to be no more than a few Kelvins. Thus we can usually neglect the temperature dependence of the material parameters and we took them to be constant across the layer.

IV. STATIONARY DISTORTED STATE

After the homeotropic state looses stability via a stationary bifurcation (at not too large angle of incidence), the director settles in a stationary distorted state. One obtains the stationary z-dependent reorientation of the director by variation of the free energy density (1) with $\mathbf{n}$ defined in terms of the angles θ, φ. This gives us two ordinary second-oder differential equations for $\theta(z)$ and $\varphi(z)$ (now these angles can be of arbitrary magnitude). We will not display them here because they are long and are obtained straightforwardly.

These equations contain the field components which obey Maxwell's equations (3). It is convenient to write (3) using the Oldano formalism [11]. Following [12] we write the matrix D (see (5)) as $\mathsf{D} = \mathsf{D_0} + \mathsf{D_z}(z)$, where

$$\mathsf{D_0} = \begin{pmatrix} 0 & 1-\frac{s_0^2}{e_\perp+e_a} & 0 & 0 \\ e_\perp & 0 & 0 & 0 \\ 0 & 0 & 0 & 1 \\ 0 & 0 & e_\perp - s_0^2 & 0 \end{pmatrix} \qquad (12)$$

and $e_\perp = \varepsilon_\perp + i\gamma_\perp$, $e_a = \varepsilon_a + i\gamma_a$. The matrix $\mathsf{D_z}$ contains the z-dependent angles θ and φ. It is convenient

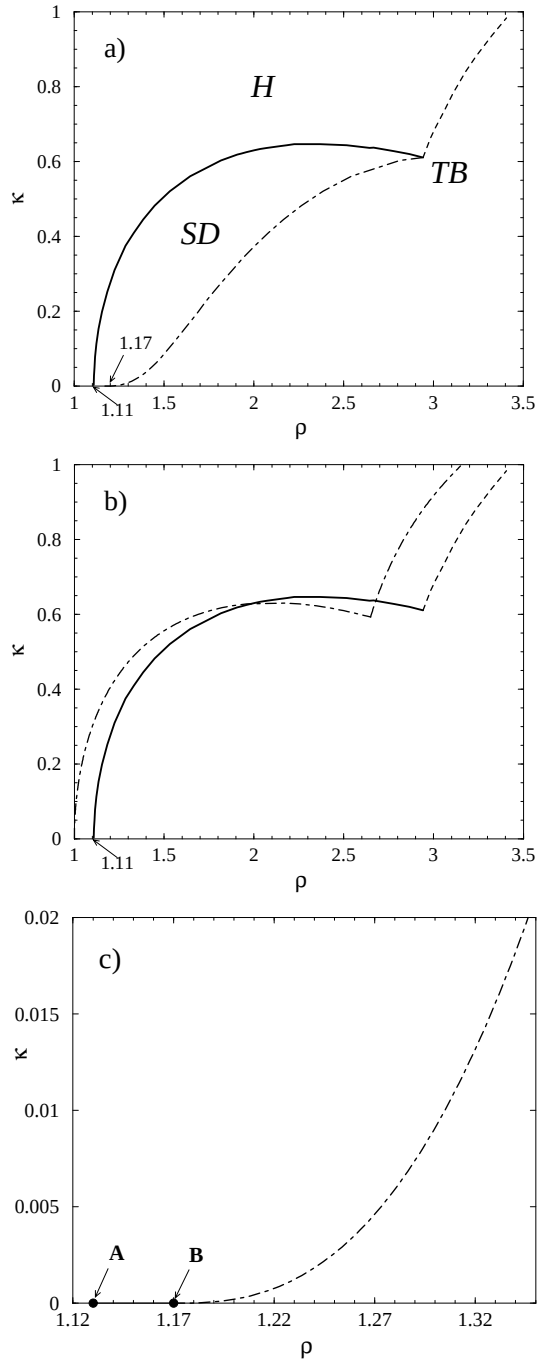


FIG. 2: a) Stability diagram of the homeotropic and stationary distorted states in the (κ, ρ) plane. H is the region of the homeotropic state. *SD* is the region of the stationary distorted state bounded toward large ρ by the secondary Hopf bifurcation (dash-dotted line). *TB* is the Takens-Bogdanov point. b) Solid and dashed lines correspond to those in Fig. 2a. The dot-dashed lines are obtained when the absorption effect is neglected. c) The secondary instability for small angles of incidence. Points A and B show the instabilities of the stationary distorted state for perpendicular incidence of the light with $n_x(z) = 0$ and $n_x(z) \neq 0$ correspondingly.

to introduce a representation in terms of eigenfunctions of D_0. The eigenvalue problem $\mathsf{D}_0\bar{\alpha}_i = a_i\bar{\alpha}_i$ is solved by the eigenvalues

$$a_2 = -a_1 = \sqrt{e_\perp - s_0^2},$$
$$a_4 = -a_3 = \sqrt{\frac{(e_\perp + e_a - s_0^2)e_\perp}{e_\perp + e_a}} \qquad (13)$$

and eigenvectors

$$\bar{\alpha}_{1,2} = \begin{pmatrix} 0 \\ 0 \\ \mp 1/a_2 \\ 1 \end{pmatrix} \quad , \quad \bar{\alpha}_{3,4} = \begin{pmatrix} \mp a_4/e_\perp \\ 1 \\ 0 \\ 0 \end{pmatrix} \qquad (14)$$

We introduce the metric tensor

$$\mathsf{M} = \begin{pmatrix} 0 & 1 & 0 & 0 \\ 1 & 0 & 0 & 0 \\ 0 & 0 & 0 & 1 \\ 0 & 0 & 1 & 0 \end{pmatrix} \qquad (15)$$

to define a scalar product between these vectors. With such a metric the eigenvectors are orthogonal to one another: $\bar{\alpha}_i^T\mathsf{M}\bar{\alpha}_j = \delta_{ij}N_i$, where N_i is the "norm" of vector $\bar{\alpha}_i$. The matrix D_0 is expressed by means of the vectors $\bar{\alpha}_i$ as $\mathsf{D}_0 = \sum_i (a_i/N_i)\bar{\alpha}_i\bar{\alpha}_i^T\mathsf{M}$. The four vectors $\bar{\alpha}_i$ give the polarization of four "proper" waves that propagate inside the layer without changing their state of polarization in the case of homeotropic alignment. The magnitudes of a_i give the indices of refraction of these waves. Two of these vectors $\bar{\alpha}_1$ ($\bar{\alpha}_2$) correspond to backward (forward) propagating ordinary waves and the other two $\bar{\alpha}_3$ ($\bar{\alpha}_4$) correspond to backward (forward) propagating extraordinary waves. The contribution of the backward waves is negligibly small because the dielectric properties of the nematic change little on the spatial scale of the wavelength [12]. Thus we can expand $\bar{\Psi}(z)$ as follows

$$\bar{\Psi}(z) = b_2(z)e^{ik_0a_2z}\bar{\alpha}_2 + b_4(z)e^{ik_0a_4z}\bar{\alpha}_4 \qquad (16)$$

and write (3) in terms of the amplitudes $b_2(z)$ and $b_4(z)$:

$$\begin{cases} \frac{db_2}{dz} = \frac{ik_0}{N_2}\left[P_{22}(z)b_2 + b_4e^{-ik_0(a_2-a_4)z}P_{24}(z)\right] \\ \frac{db_4}{dz} = \frac{ik_0}{N_4}\left[P_{44}(z)b_4 + b_2e^{-ik_0(a_4-a_2)z}P_{42}(z)\right], \end{cases} \qquad (17)$$

where $P_{kj}(z) = \bar{\alpha}_k^T\mathsf{M}\mathsf{D}_\mathsf{z}(z)\bar{\alpha}_j$ are the matrix elements of D_z between the eigenvectors:

$$P_{22} = \frac{e_a e_\perp \cos(\theta)^2 \sin(\varphi)^2}{a_2^2(e_\perp + e_a\cos(\theta)^2\cos(\varphi)^2)},\ P_{24} = P_{42} = \frac{[a_4\sin(\theta) - \cos(\theta)\cos(\varphi)s_0]\sin(\varphi)\cos(\theta)e_a}{a_2(e_\perp + e_a\cos(\theta)^2\cos(\varphi)^2)},$$
$$P_{44} = \frac{e_a\left[(a_4\sin(\theta)^2 - \sin(2\theta)\cos(\varphi)s_0)(e_\perp + e_a)a_4 + e_\perp s_0^2(\cos(\theta)^2\cos(\varphi)^2 - 1)\right]}{e_\perp(e_\perp + e_a)(e_\perp + e_a\cos(\theta)^2\cos(\varphi)^2)} \quad (18)$$

The advantage of the system (17) is that we now have only two equations for the "slow" amplitudes $b_2(z)$ and $b_4(z)$. So, we have a system of coupled ordinary differential equations for $\theta(z)$, $\varphi(z)$, $b_2(z)$ and $b_4(z)$ with boundary conditions $\theta|_{z=0,L} = \varphi|_{z=0,L} = 0$, and initial conditions $b_2|_{z=0} = A_0$, $b_4|_{z=0} = 0$. Here A_0 can be related to the normalized intensity ρ defined in the previous section: $A_0 = \sqrt{8\pi^3\left(\varepsilon_a + \varepsilon_\perp\right)\left(\varepsilon_\perp - s_0^2 + i\gamma_\perp\right)\rho/(\varepsilon_a\varepsilon_\perp\eta)}$.

The system of "nematic+field" equations (with boundary conditions) is invariant under the transformation $[\theta, \varphi, E_x, E_y] \to [\theta, -\varphi, E_x, -E_y]$ owing to the reflection symmetry with respect to the y direction. Since the primary instability breaks this symmetry, two different distorted states exist, which are mutual images under this transformation. For perpendicular incidence of the light there is an additional reflection symmetry with respect to the x direction and, as a consequence, the system of equations is also invariant under the transformation $[\theta, \varphi, E_x, E_y] \to [-\theta, \varphi, -E_x, E_y]$.

The system of equations can only be solved numerically. For this purpose we introduced the new variables $d\theta/dz, d\varphi/dz$ to transform our set of equations to a system of six first-oder equations which was solved by the shooting method. To guarantee that we obtain the solution which originates from the homeotropic state we started with intensities only slightly above the threshold. Then, we increased ρ slightly and used the values of $d\theta/dz|_{z=0}$, $d\varphi/dz|_{z=0}$ obtained in the previous step as an initial guess. This procedure allowed us to derive the profiles $\theta(z)$, $\varphi(z)$, $b_2(z)$ and $b_4(z)$ for any κ and ρ above threshold.

The director and field distributions for $\rho = 2.0$ and $\beta_0 = 11^\circ$ ($\kappa = 0.375$) are shown in Figs. 3,4. In the next section we will show that for $\kappa = 0.375$ the stationary distorted state becomes unstable at $\rho_c = 2.01$, thus these figures represent the state slightly below the secondary instability.

V. STABILITY ANALYSIS OF THE STATIONARY DISTORTED STATE

Next we have performed a linear stability analysis of the distorted stationary state with respect to spatially periodic perturbations in the plane of the nematic layer. We write

$$\mathbf{n} = \mathbf{n}_0(z) + \delta\mathbf{n}(x,y,z,t) = \mathbf{n}_0(z) + \delta\mathbf{n}(z)e^{\sigma t + i(qx+py)}, \quad \bar{\Psi} = \bar{\Psi}_0 + \bar{\Psi}_1 = \sum_{k=2,4}(b_k(z) + \delta b_k(z)e^{\sigma t + i(qx+py)})e^{ik_0 a_k z}\bar{\alpha}_k, \quad (19)$$

where $\delta\mathbf{n}$ and δb_k are small spatially periodic perturbation with wavenumbers q and p; σ is the growth rate.

From the equation $\mathbf{n}^2 = 1$ follows that $\mathbf{n_0}\delta\mathbf{n} = \mathbf{0}$. Thus there are only two independent components of $\delta\mathbf{n}$. We obtained two linear equations for $\delta n_x(z)$ and $\delta n_y(z)$ which contain $\delta n_x(z)$, $\delta n_y(z)$ itself, their z derivatives up to second oder and $\delta b_{2,4}(z)$ with complicated coefficients depending on the stationary distorted state $\mathbf{n}_0(z), b_{2,4}(z)$. Also, we decomposed the matrix D (see (5)) as $\mathsf{D} = \mathsf{D_0} + \mathsf{D_z(z)} + \mathsf{D_1}(\delta\mathbf{n})$, where the matrices $\mathsf{D_0}, \mathsf{D_z(z)}$ correspond to the stationary state and were defined in the previous section, and the matrix $\mathsf{D_1}(\delta\mathbf{n})$ depends linearly on $\delta\mathbf{n}$. After linearization of (3) the equations for $\delta b_{2,4}$ can be obtained:

$$\begin{cases} \frac{d(\delta b_2(z))}{dz} = \frac{ik_0}{N_2}\left(\delta b_2 P_{22} + \delta b_4 e^{ik_0(a_4-a_2)z}P_{24} + b_2 P_{22}^{(1)} + b_4 e^{ik_0(a_4-a_2)z}P_{24}^{(1)}\right) \\ \frac{d(\delta b_4(z))}{dz} = \frac{ik_0}{N_4}\left(\delta b_2 e^{ik_0(a_2-a_4)z}P_{24} + \delta b_4 P_{44} + b_2 e^{ik_0(a_2-a_4)z}P_{24}^{(1)} + b_4 P_{44}^{(1)}\right), \end{cases} \quad (20)$$

where $P_{kj}^{(1)} = \bar{\alpha}_k^T \mathsf{M}\mathsf{D_1}\bar{\alpha}_j$ are the matrix elements of $\mathsf{D_1}$ with respect to the eigenvectors (14) and the P_{kj} were defined in (18).

We have linearized the equation (3) substituting ψ in the form (19). In principle we should have started from Maxwell's equations because the field perturbations contain x, y dependence. However this is a very good approximation because the corrections are of the oder q/k_0, $p/k_0 << 1$.

To solve the eigenvalue problem for σ we expand

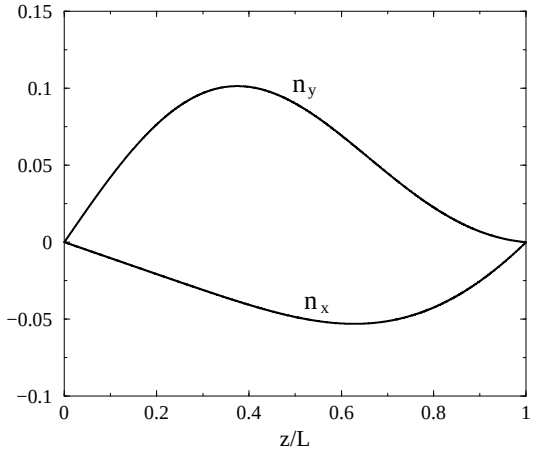


FIG. 3: Profiles of the director components n_x, n_y for the stationary distorted state at $\rho = 2.0$ and $\beta_0 = 11^\circ$ ($\kappa = 0.375$).

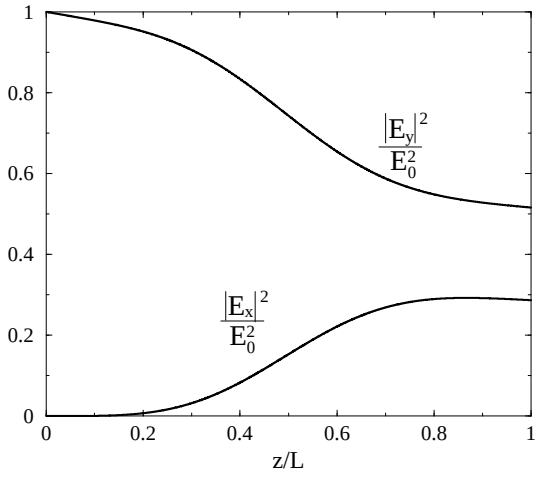


FIG. 4: Distortion of the field components inside the nematic layer for the stationary distorted state ($\rho = 2.0$, $\beta_0 = 11^\circ$). E_z is small compared to E_x, E_y and is not depicted; E_0 is the amplitude of the incident electric field.

$\delta n_{x,y}(z)$, $\delta b_{2,4}(z)$ with respect to z in systems of functions which satisfy the boundary conditions (Galerkin method). For $\delta\mathbf{n}$ the boundary conditions are $\delta n_{x,y}|_{z=0,L} = 0$, thus we write $\delta\mathbf{n}=\sum_k \mathbf{A}_k \sin(\pi k z/L)$. Clearly the boundary conditions for the perturbations of the field amplitudes are $\delta b_{2,4}|_{z=0} = 0$. One can see that at $z = 0, L$ the r.h.s. of the system (20) vanishes so one also has $d(\delta b_{2,4})/dz|_{z=0,L} = 0$. Therefore we used the expansion $\delta\mathbf{b} = \sum_n \mathbf{B}_n \sin^2(\pi n z/(2L))$. This set of functions is complete but not orthogonal. We have to truncate these expansions to a finite number of modes.

We have solved the eigenvalue problem numerically to find the neutral surface $\rho_0(q, p)$ (for given angle β_0) which is defined by the condition $Re(\sigma(q, p)) = 0$. The number of Galerkin modes was chosen such that the accuracy of the calculated eigenvalues was better than 0.1% (we took six modes for $\delta\mathbf{n}$ and forty modes for $\delta\mathbf{b}$). The minimum of this surface gives the critical intensity ρ_c=$\min_{q,p} \rho_0(q, p)$ and the critical wavevector (q_c, p_c). Since $\Omega_c = Im(\sigma)$ turned out to be nonzero at the minimum, the instability corresponds to a Hopf bifurcation. The branch of the secondary Hopf instability is depicted as the dash-dotted line in Fig. 2a and for small angles of incidence in Fig. 2c. It is interesting to note the following tendencies: as the incident angle β_0 increases the critical intensity also increases, but the director and field deformations at the secondary instability decrease.

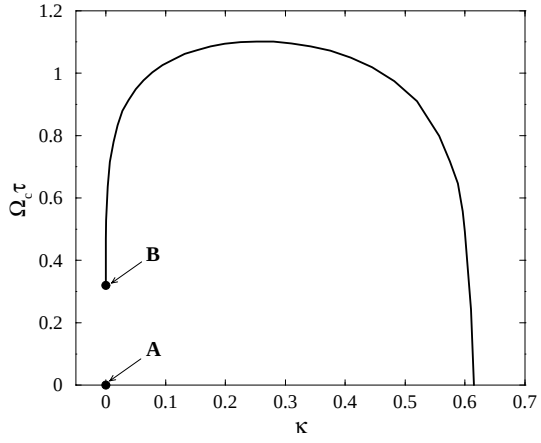


FIG. 5: Dimensionless Hopf frequency $\Omega_c\tau$ for the secondary instability versus κ. Points A and B are the Hopf frequencies at points A and B depicted in Fig. 2 c).

The dimensionless Hopf frequency $\Omega_c\tau$ (τ is defined in section III) versus κ is shown in Fig. 5. Figure 6 shows a typical contour plot of the neutral surface $\rho_0(q, p)$. The point $(q_c L, p_c L)$ in this figure is the minimum of the surface and as is seen the bifurcation is inhomogeneous with some critical vector $(q_c, p_c) \neq \vec{0}$. This means that travelling waves are expected to appear. ρ_c is only slightly below the homogeneous threshold $\rho_0(q = 0, p = 0)$, which was calculated before for the pure LC [12, 13].

As was pointed out in section IV, for nonzero β_0 there are two symmetry-degenerate stationary distorted states. Clearly the two neutral surfaces are related by changing p to $-p$ and the critical wave vectors will be (q_c, p_c) and $(q_c, -p_c)$. Thus two different travelling waves with critical vectors $(q_c, \pm p_c)$ can be realized depending on which stationary state will be selected after the homeotropic state loses stability.

An interesting situation arises in the limit of normal incidence. One might expect that for $\beta_0 \to 0$ the wavenumber $q_c \to 0$, since in this limit the external symmetry breaking in the x direction vanishes. However, this turned out not to be the case. The reason is that then another stationary instability that spontaneously breaks x-reflection symmetry intervenes the primary and the Hopf bifurcation. For the parameters of our computation one has $\rho_{th} = 1.11$, $\rho_{c1} = 1.13$ (point A in Fig.

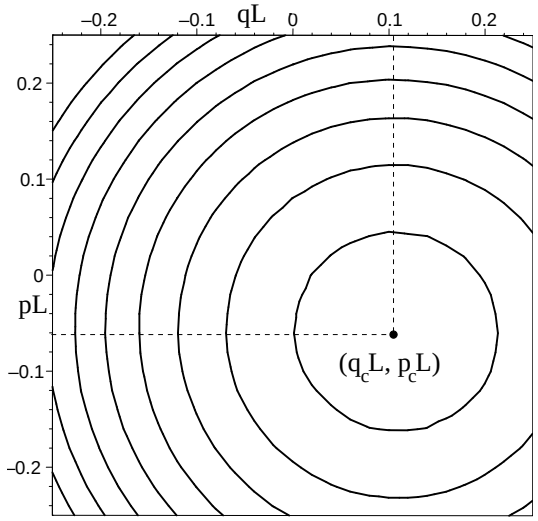


FIG. 6: Contour lines for the surface $\rho(p,q)$ correspond to $\beta_0 = 11^\circ$ ($\kappa = 0.375$). The critical intensity is $\rho_c = 2.01$ with the critical wavevector $(q_cL, p_cL) = (0.11, -0.06)$; $\rho_0(q = 0, p = 0) - \rho_c = 1.5 \cdot 10^{-3}$.

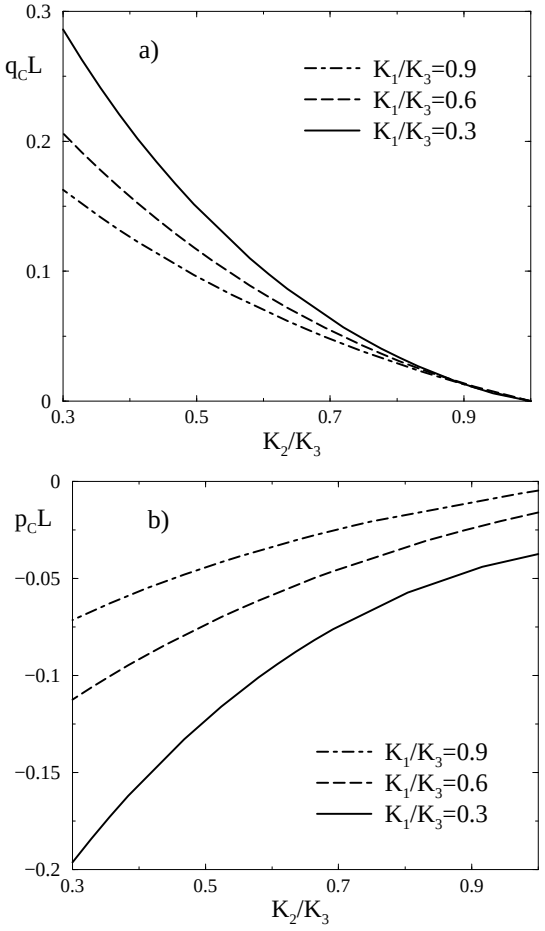


FIG. 7: Critical wavenumbers q_c, p_c versus K_2/K_3 for different ratios K_1/K_3 ($\beta_0 = 11^\circ$).

2c) and $\rho_{c2} = 1.17$ (point B in Fig. 2c). One now has four symmetry-degenerate states and consequently four traveling waves with critical wave vectors $(\pm q_c, \pm p_c)$. In some further investigations we have changed the ratios between the elastic constants keeping other material parameters constant and saw the following tendency: the larger the anisotropy of the constants, the deeper the minimum of the surface becomes and the larger the magnitudes of the critical wavenumbers (see Fig. 7a,b). The absolute error of the dimensionless critical wavenumbers q_cL, p_cL depicted in this figure is less than 10^{-2}. In the one-constant approximation the bifurcation is homogeneous ($q_c, p_c = 0$) for any κ. This latter can be easily proved analytically. Perturbation theory can be used to investigate q, p dependence of the critical eigenvalue of an arbitrary stationary state. The calculations shows, that the perturbation of the eigenvalue is $\sim p^2 + q^2$.

From Fig. 7a,b one can see that $q_cL, p_cL \sim 0.1$. This means that the period of the structure $2\pi/q_c,\ 2\pi/p_c \sim 60L = 0.3\ cm$. Thus in an experiment the spot size of the light must be rather large in oder to observe the travelling waves.

Finally we remark on the behaviour of the system in the nonlinear regime above the Hopf bifurcation. This system without transverse degrees of freedom has been studied extensively, and various regimes of complex behaviour have been discovered. The bifurcation studied in this work marks the transition to simple periodic oscillations in the system without transverse degrees of freedom, which is the first step towards complex behaviour. In models [12, 13] and simulations [14], a gluing bifurcation was found above the secondary Hopf instability, which is a homoclinic bifurcation that restores the symmetry broken by the Freedericksz transition. This gluing bifurcation was recently observed experimentaly [15]. After this first gluing, complex nonlinear behaviour and eventually chaos was observed in both theory, simulation and experiment [16]. An analogous gluing bifurcation should exist also in the case of the spatially extended system.

The behaviour of the system in the vicinity of this gluing bifurcation, can, however be radically different from what was observed in the experiment [15]. In the spatially constrained system (i.e. the director oscillation induced by a narrow beam as observed in the experiments) one observes stochastic behaviour in the vicinity of the first gluing only as a consequence of experimental noise. It has been shown, however, [17] that any spatially extended system, which possesses a homogeneous limit cycle (which is stable with respect to homogeneous perturbations) becomes unstable as it approaches a homoclinic bifurcation. This instability is either a phase instability, or a finite-wavelength period-doubling instability. On these grounds one can expect to observe very complicated behaviour (probably spatio-temporal chaos) in our system already at the threshold intensity of the first gluing. As opposed to the previous case, this would

be true deterministic chaos, not merely stochasticity due to noise.

VI. CONCLUSION

We have found the threshold of the LIFT for the homeotropic state and the threshold of the secondary instability of the stationary distorted state in a nematic LC, including the dye-doped case, for different incident angles of the light. In particular we have demonstrated that the stationary distorted state loses stability in an inhomogeneous Hopf bifurcation with some nonzero critical wavenumber that leads to the formation of travelling waves in the plane of the layer.

Our result demonstrates a general feature of Hopf bifurcations in spatially extended systems with broken reflection symmetry, as is the case in the LIFT-distorted state. Except for special cases, like those where the reflection symmetry can be restored by going into a moving frame, the neutral surface exhibits the signature of the broken symmetry. Consequently, at $q_c = p_c = 0$ the neutral surface does not have a stationary point and thus cannot have a minimum. This general feature was apparently first noted in the context of reaction-diffusion systems [18].

VII. ACKNOWLEDGMENTS

We wish to thank A.P. Krekhov for helpful discussions. This work was supported by DFG grant N° KR690/16-1.

[1] N. V. Tabiryan, A. V. Sukhov and B. Ya. Zel'dovich, Mol. Cryst. Liquid Cryst. **136**, 1-140 (1985).
[2] F. Simoni, *Nonlinear optical properties of liquid crystals* (World Scientific, Singapore, 1997).
[3] F. Lonberg and R. B. Meyer, Phys. Rev. Lett. **55**, 718 (1985).
[4] D. W. Allender, R. M. Hornreich and D. L. Johnson, Phys. Rev. Lett. **59**, 2654 (1987).
[5] Istvan Janossy, J. Nonlin. Opt. Phys. Mat. **8**, 361 (1999).
[6] L. Marrucci, D. Paparo, P. Maddalena, E. Massera, E. Prudnikova, and E. Santamato, J. Chem. Phys **107**, 9783 (1997).
[7] P. G. de Gennes and J. Prost, *The physics of liquid crystals* (Clarendon press, Oxford, 1993).
[8] N.V. Tabiryan, A.L. Tabiryan-Murazyan, V. Carbone, G. Cipparrone, C. Umeton, C. Versace, T. Tschudi, Optics Comm. **154**, 70 (1998).
[9] A. Buka and L. Kramer, *Pattern formation in liquid crystals* (Springer, 1995).
[10] I. Janossy and T. Kosa, Mol. Cryst. Liq. Cryst. **207**, 189 (1991).
[11] C. Oldano, Phys. Rev. A **40**, 6014 (1989).
[12] G. Demeter, Phys. Rev. E **61**, 6678 (2000).
[13] G. Demeter and L. Kramer, Phys. Rev. Lett. **83**, 4744 (1999).
[14] G. Demeter and L. Kramer, Phys. Rev. E **64**, 020701(R) (2001).
[15] V. Carbone, G. Cipparrone, and G. Russo, Phys. Rev. E **63**, 051701 (2001).
[16] G. Cipparrone, V. Carbone, C. Versace, C. Umeton, R. Bartolino and F. Simoni, Phys. Rev. E **47**, 3741 (1993).
[17] M. Argentina, P. Coullet and E. Risler, Phys. Rev. Lett. **86**, 807 (2001); P. Coullet, E. Risler, N. Vandenberghe, J. Stat. Phys. **101**, 521 (2000).
[18] A. B. Rovinsky and M. Menzinger, Phys. Rev. Lett. **69**, 1193 (1992); **70**, 778 (1993).